Charge transport in molecular junctions: From tunneling to hopping with the probe technique

Michael Kilgour[1] and Dvira Segal[1, a)]
Chemical Physics Theory Group, Department of Chemistry, University of Toronto, 80 St. George Street Toronto, Ontario, Canada M5S 3H6

(Dated: 5 September 2018)

We demonstrate that a simple phenomenological approach can be used to simulate electronic conduction in molecular wires under thermal effects induced by the surrounding environment. This "Landauer-Büttiker's probe technique" can properly replicate different transport mechanisms: phase coherent nonresonant tunneling, ballistic behavior, and hopping conduction, to provide results consistent with experiments. Specifically, our simulations with the probe method recover the following central characteristics of charge transfer in molecular wires: (i) The electrical conductance of short wires falls off exponentially with molecular length, a manifestation of the tunneling (superexchange) mechanism. Hopping dynamics overtakes superexchange in long wires demonstrating an ohmic-like behavior. (ii) In off-resonance situations, weak dephasing effects facilitate charge transfer. Under large dephasing the electrical conductance is suppressed. (iii) At high enough temperatures, $k_B T/\epsilon_B > 1/25$, with ϵ_B as the molecular-barrier height, the current is enhanced by a thermal activation (Arrhenius) factor. However, this enhancement takes place for both coherent and incoherent electrons and it does not readily indicate the underlying mechanism. (iv) At finite-bias, dephasing effects impede conduction in resonant situations. We further show that memory (non-Markovian) effects can be implemented within the Landauer-Büttiker's probe technique to model the interaction of electrons with a structured environment. Finally, we examine experimental results of electron transfer in conjugated molecular wires and show that our computational approach can reasonably reproduce reported values to provide mechanistic information.

I. INTRODUCTION

Understanding of charge transport mechanisms in single-molecule junctions is essential for the realization of molecular electronic devices, as well as for elucidating many processes in chemistry, biology, and condensed phase physics. Examples include charge transfer in DNA[1,2], a process which plays a crucial role in mutagenesis and carcinogenesis, electron transfer reactions[3–5], and electron correlation effects at the nanoscale, such as in quantum dots and molecular junctions[6–8].

Experiments probing electron transfer (ET) rates in donor-acceptor DNA molecules[9–12], self-assembled monolayers and single-molecule wires[13–31] have demonstrated the central role of two limiting transport mechanisms: phase coherent nonresonant tunneling (superexchange) and incoherent thermally-activated hopping. Direct tunneling, a single step transition, dominates transport in short wires, but becomes unlikely at large molecular lengths as tunneling rates decrease exponentially with length. In contrast, long-range electron transfer can take place when the transport process is broken into multiple steps, with the electron (or hole), transiently localized on molecular sites, hopping between them. Furthermore, in molecular wires bridging two voltage-biased electrodes, "field emission", (Fowler-Nordheim tunneling) behavior develops when the applied voltage bias transforms the tunneling barrier from a rectangular form into a triangular shape[20,24].

In an effort to explain experimental results, and moreover, predict molecular electronic functionality, a plethora of theoretical and computational methodologies were developed, aiming to explore the role of environmental effects (internal molecular motion or the surrounding matrix) on molecular conduction. These tools can be roughly grouped into two classes: (i) microscopic-physical modelings which are valuable for small systems, and (ii) phenomenological descriptions, compromising the completeness and exactness of the model to enable large-scale calculations. The first type of approaches corresponds to models in which molecular vibrations, and other many-body interactions such as electron-electron repulsion are explicitly included in the model Hamiltonian. The dynamics and steady-state properties of the system can then be analyzed by a variety of treatments. A non-exhaustive list, focusing on vibrational effects in molecular conduction, includes density operator approaches[32,33], Green's function tools[34] and path integral simulations[35–37]. Since the vibrational degrees of freedom and/or electron-electron interactions are explicitly incorporated in such treatments, simulations are restricted to minimal models with a single molecular electronic state, or a pair of states. The Anderson-Holstein model takes into account a single electronic level and a particular vibration. Other common modelings consider only two molecular orbitals, HOMO and LUMO, as decisive for electronic conduction[34].

Complementing minimal-microscopic approaches, it is beneficial to establish effective-phenomenological methodologies for electronic conduction with a more favorable scaling with molecular size. The Lindblad for-
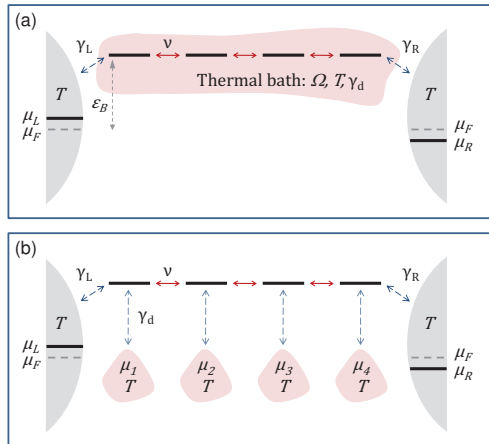
FIG. 1. (a) A molecular wire with N electronic sites (inter-site tunneling v and bridge height ϵ_B) coupled to a thermal environment, represented by the shaded region surrounding the electronic states. The thermal bath, including molecular and external vibrational degrees of freedom, is characterized by its temperature T, spectral density function with a cutoff frequency Ω and electron-vibration coupling strength γ_d. (b) In this work we introduce the environment in a phenomenological manner by using the probe technique, by attaching fictitious metal terminals to electronic sites. The figure illustrates voltage probes, characterized by their temperature and chemical potentials which are determined such that there is zero net charge current to each probe.

malism, Redfield theory, and other kinetic equations, are examples of such approaches[5,38]. In these treatments the interaction of electrons with environmental degrees of freedom is incorporated into the dynamics via decoherence and dissipation rates which are introduced into the equations of motion for the reduced density matrix. Variants of such projection operator techniques have been employed extensively in the literature to model electron, proton, phonon, and exciton dynamics in condensed phases[4,5]. In donor-bridge-acceptor electron transfer (DBA-ET) processes, such methods have proven useful for describing, in a unified manner, both the tunneling and the incoherent-hopping regime[39–48]. More recent works rigorously examined the consistency of these effective treatments for describing steady-state characteristics[49–51], and applied kinetic approaches to predict electronic functionality[52,53].

A distinct phenomenological route to implement decoherence and inelastic effects was introduced by Büttiker in Ref.[54]. In this "Landauer-Büttiker's probe" (LBP) approach the non-interacting Hamiltonian is augmented by probe terminals in which electrons lose their phase memory and exchange energy with probes' degrees of freedom. This technique, so far mostly employed in mesoscopic physics[55], e.g. to study heat to work conversion efficiency in thermoelectric devices[56–58] and magnetotransport in quantum dot systems[59,60], is particularly appealing: It allows one to model phase breaking

processes e.g. in quantum dots, while using the Landauer non-equilibrium Green's function (NEGF) computational tool[6–8,61]. Beyond electronic conduction, the LBP technique has been adopted to explore heat transport and thermal rectification in linear chains[62–68] and two-dimensional constrictions[69].

The LBP method had proved itself predictive in studies of charge and heat transport in mesoscopic physics. Can it appropriately describe environmental effects on electronic conduction in molecular junctions? Recently, this technique has been applied to explore the role of decoherence on quantum interference in molecular conduction[70] and to examine the connection between charge transfer kinetics and steady state currents[71], showing that it can provide both the tunneling mechanism for short bridges, and a "soft"-ohmic distance dependence for longer chains. However, a careful exploration of the LBP method in molecular electronic configurations is missing. Our objective here is to employ the LBP technique and examine whether it can yield results consistent with our comprehensive knowledge of environmental-assisted electron transfer effects in molecular electronic junctions. Particularly, the technique should depict the turnover in transport, from tunneling to hopping, with increasing molecular size, temperature, and dephasing rates.

Another objective of this work has been to develop an approximate analytic expression for hopping conduction in molecular junctions. Several works have undertaken this task in a donor-bridge-acceptor configurations to construct the *electron transfer rate*, a related quantity[42,44–47,72,73]. However, few theoretical studies had considered this problem in a metal-molecule-metal setup[28,43,74–76], which differs fundamentally from the DBA-ET situation: While in the latter case the initial condition places all electrons in the donor state with a given energy, in a metal-molecule-metal experiment many electronic states in the metals contribute, and electrons, with a thermal distribution of energies, determine the electronic conductance.

Simulations presented in this work confirm that the LBP method can properly emulate experimentally-observed characteristics of molecular electronic conduction in wires with a tunable "dephasing strength" parameter, characterizing the strength of electron-environment interactions. Based on our simulations we suggest an analytic expression which describes hopping conduction in molecular wires. The Landauer-NEGF technique is nowadays the leading method in modeling the operation of *phase-coherent* molecular electronic devices[6–8,61]. Particularly, recent measurements of molecular thermopower (see for example Refs.[77,78]) and heat dissipation in nanojunctions[79] were explained using this method. By establishing here the appropriateness of the LBP treatment in molecular electronic conduction problems we advocate for the natural generalization of the Landauer-NEGF technique to incorporate environmental-assisted transport effects by including LBPs.

This paper is organized as follows. In Sec. II we

present the wire model and the probe technique. Sec. III summarizes transport mechanisms in molecular junctions. In Sec. IV we present numerical simulations under low applied voltage. Based on observations, we construct an analytic expression for bath-assisted molecular electronic conduction. The behavior of the junction under large applied voltage is described in Sec. V. In Sec. VI we apply our computational method and compare findings to experimental results for transport in long conjugated molecules. We conclude in Sec. VII.

In this work we interchangeably refer to the molecular system as a "molecular wire", "molecular junction", or, a "molecular bridge". Identifying the system as a "wire" emphasizes that molecules under consideration include repeating units, and that they are capable of transferring charges over long distances. The term "junction" highlights the geometry: the molecule is placed between two metal electrodes, distinguishing it from the DBA situation. The title "bridge" describes the structure assumed: We study situations in which molecular orbitals relevant for transport lie above the Fermi energies of the two electrodes. Molecular electronic degrees of freedom are coupled to environmental coordinates (here, mimicked by probes). The environment may correspond to internal molecular vibrations or the solvent's degrees of freedom (we exclude the metals' electrons from this definition). We collectively refer to these nuclear coordinates as a "thermal bath", "environment", or "surrounding", assumed to be maintained at the temperature of the metals.

II. MODEL AND METHOD

A. Model Hamiltonian

We consider a molecule bridging metal electrodes with the Hamiltonian

$$\hat{H} = \hat{H}_W + \hat{H}_L + \hat{H}_R + \hat{H}_T + \hat{H}_P + \hat{V}_P. \quad (1)$$

It comprises the molecular wire $\hat{H}_W$, two electrodes $\hat{H}_L$ and $\hat{H}_R$, and a coupling Hamiltonian $\hat{H}_T$ allowing charge transfer between the two leads and the wire. We further introduce (in a phenomenological manner) dephasing and inelastic effects for electrons on the molecule. This is achieved by attaching local reservoirs ($\hat{H}_P$) to each site in the wire (coupling Hamiltonian $\hat{V}_P$), see Fig. 1. The molecular wire includes N single-level sites of energy ϵ_n,

$$\hat{H}_W = \sum_{n=1}^{N} \epsilon_n \hat{c}_n^\dagger \hat{c}_n + \sum_{n=1}^{N-1} v_{n,n+1} \hat{c}_n^\dagger \hat{c}_{n+1} + h.c. \quad (2)$$

Here, $\hat{c}_n^\dagger$ ($\hat{c}_n$) are fermionic creation (annihilation) operators of electrons on each site in the wire, the parameters $v_{n,n+1}$ are the inter-site tunneling energies. In what follows we consider molecules made of identical building blocks, thus we introduce the short notation $\epsilon_B = \epsilon_n$ and

$v = v_{n,n+1}$. The metal electrodes are modeled by a Fermi sea of noninteracting electrons,

$$\hat{H}_\nu = \sum_k \epsilon_{\nu,k} \hat{a}_{\nu,k}^\dagger \hat{a}_{\nu,k}, \quad \nu = L, R. \quad (3)$$

$\hat{a}_{\nu,k}^\dagger$ ($\hat{a}_{\nu,k}$) are fermionic creation (annihilation) operators of electrons with momentum k in the ν lead. Electrons can tunnel from the L (R) metal to site 1 (N),

$$\hat{H}_T = \sum_k g_{L,k} \hat{a}_{L,k}^\dagger \hat{c}_1 + \sum_k g_{R,k} \hat{a}_{R,k}^\dagger \hat{c}_N + h.c. \quad (4)$$

In the absence of the probes, this Hamiltonian dictates phase-coherent electron dynamics, reflected e.g., by a tunneling behavior[5]. We now include N probes, additional metal electrodes

$$\hat{H}_P = \sum_{n=1}^{N} \sum_k \epsilon_{n,k} \hat{a}_{n,k}^\dagger \hat{a}_{n,k}. \quad (5)$$

The nth probe can exchange particles with the nth site of the molecular wire,

$$\hat{V}_P = \sum_{n=1}^{N} \sum_k g_{n,k} \hat{a}_{n,k}^\dagger \hat{c}_n + h.c. \quad (6)$$

Here $\hat{a}_{n,k}^\dagger$ ($\hat{a}_{n,k}$) are fermionic creation (annihilation) operators for an electron in the $n = 1, 2, ..., N$ probe with momentum k, $g_{n,k}$ are the tunneling energies from the nth molecular site into the nth probe. To eliminate charge leakage processes from the molecular wire into the probes we enforce certain conditions on conduction. In Sec. II B we describe in detail two such constrains, the "dephasing probe" and the "voltage probe".

B. Büttiker's Probes technique

The Landauer approach provides a simple-exact description of phase coherent quantum transport[6]. Given its simplicity, it is appealing to use it beyond the coherent limit. Indeed, as was shown in Ref.[54], one can implement (elastic and inelastic) scattering of electrons with other degrees of freedom, possibly phonons, photons, and other electrons, by introducing additional terminals (probes) into the model system. The key point here is that the parameters of these terminals, essentially their local charge distributions, should be set in a self-consistent way such that there is no net (average) particle current between the physical system of interest and the probes.

The probe technique can be implemented under different self-consistent conditions, allowing us to craft electron scattering processes: elastic dephasing effects are implemented via the "dephasing probe", while dissipative inelastic effects are introduced through the "voltage probe". Further, dissipation-less inelastic scattering processes can be admitted by requiring the net average fluxes of particles and heat between the probe terminal and the

system to vanish, termed as the "temperature-voltage probe". These probes can be operated in the linear response regime, as well as far from equilibrium[80].

Below we employ ν to identify the L and R (physical) metal electrodes to which the molecule is connected. We count the probe terminals with the index n and use α to identify all leads, the two metal electrodes $\nu = L, R$ and the $n = 1, 2, .., N$ probes.

Since the model Hamiltonian does not include interactions, its charge transfer characteristics can be described with the Landauer-Büttiker formalism[6]. The total current leaving the L contact is given by

$$I_L = \frac{e}{2\pi\hbar} \sum_\alpha \int_{-\infty}^\infty \mathcal{T}_{L,\alpha}(\epsilon) [f_L(\epsilon) - f_\alpha(\epsilon)] d\epsilon. \quad (7)$$

This expression should be multiplied by a factor of 2 to account for the spin degree of freedom. Since magnetic effects are absent, $\mathcal{T}_{\alpha,\alpha'}(\epsilon) = \mathcal{T}_{\alpha',\alpha}(\epsilon)$. $f_\nu(\epsilon) = [e^{\beta(\epsilon-\mu_\nu)} + 1]^{-1}$ are the Fermi functions in the physical electrodes, given in terms of the inverse temperature $k_B T = \beta^{-1}$ and chemical potentials μ_ν. The functions $f_n(\epsilon)$ are to be determined from the probe condition.

The electrical conductance is defined as the ratio of charge current to applied voltage, $\Delta V = (\mu_L - \mu_R)/e$,

$$G = I_L/\Delta V. \quad (8)$$

This definition does not necessarily assume low voltages. One often further defines a linear response electrical conductance demanding the applied bias to be the smallest energy scale in the system, $|e\Delta V| < 1/\beta, D, \gamma_\nu, \epsilon_B, v, \gamma_d$, with γ_ν and γ_d defined after Eq. (13) and D as the bandwidth of the metal leads, the largest energy scale. In our simulations we principally work under the low-bias condition, yet for simplicity use everywhere the definition (8).

In direct analogy to Eq. (7), the net current between the nth probe and the system can be written as

$$I_n = \frac{e}{2\pi\hbar} \sum_\alpha \int_{-\infty}^\infty \mathcal{T}_{n,\alpha}(\epsilon) [f_n(\epsilon) - f_\alpha(\epsilon)] d\epsilon. \quad (9)$$

The transmission functions in Eqs. (7) and (9) are obtained from the $(N \times N)$ Green's function and the hybridization matrices[5],

$$\mathcal{T}_{\alpha,\alpha'}(\epsilon) = \text{Tr}[\mathbf{\Gamma}_\alpha(\epsilon)\mathbf{G}^\dagger(\epsilon)\mathbf{\Gamma}_{\alpha'}(\epsilon)\mathbf{G}(\epsilon)], \quad (10)$$

where the trace is performed over the N states of the molecule. The Green's function is obtained from the inverse of a tridiagonal matrix, $\mathbf{A} = [\mathbf{G}^\dagger]^{-1}$, with the matrix elements

$$\mathbf{A}_{n,n}(\epsilon) = \epsilon - \epsilon_B + \frac{i}{2}[\gamma_L(\epsilon)\delta_{n,1} + \gamma_R(\epsilon)\delta_{n,N} + \gamma_n(\epsilon)]$$

$$\mathbf{A}_{n,n\pm1}(\epsilon) = -v. \quad (11)$$

The hybridization matrices have a single nonzero value as follows,

$$[\mathbf{\Gamma}_n(\epsilon)]_{n,n} = \gamma_n(\epsilon),$$
$$[\mathbf{\Gamma}_L(\epsilon)]_{1,1} = \gamma_L(\epsilon), \quad [\mathbf{\Gamma}_R(\epsilon)]_{N,N} = \gamma_R(\epsilon), \quad (12)$$

with energies

$$\gamma_\alpha(\epsilon) = 2\pi \sum_k |g_{\alpha,k}|^2 \delta(\epsilon - \epsilon_{\alpha,k}). \quad (13)$$

We work in the wide-band limit, unless otherwise stated, and take γ_α as energy independent parameters. Below we assume that all sites in the wire are similarly affected by the probes, thus we use a single parameter to identify the probe-molecule hybridization energy, $\gamma_d = \gamma_n$. We also define the harmonic mean $\gamma = \frac{1}{2}\gamma_L\gamma_R/(\gamma_L + \gamma_R)$ as a measure for the molecule-metal coupling.

We now describe the dephasing probe and the voltage probe conditions. In the linear response regime at low enough temperatures the two probes act similarly on the molecule.

Dephasing Probe. We implement local elastic dephasing effects by forcing the *energy-resolved* particle currents, between every probe and the system, to diminish. Mathematically, we demand the integrand in Eq. (9) to nullify. This condition translates into a set of N linear equations for the functions $f_n(\epsilon)$, given in terms of the Fermi distributions at the L and R electrodes,

$$\left[\sum_{n'} \mathcal{T}_{n,n'}(\epsilon) + \mathcal{T}_{n,L}(\epsilon) + \mathcal{T}_{n,R}(\epsilon)\right] f_n(\epsilon) - \sum_{n'} \mathcal{T}_{n,n'}(\epsilon) f_{n'}(\epsilon)$$
$$= \mathcal{T}_{n,L}(\epsilon) f_L(\epsilon) + \mathcal{T}_{n,R}(\epsilon) f_R(\epsilon). \quad (14)$$

We solve this linear set repeatedly, for energies ϵ extending $-D$ to D, with D a high energy cutoff (bandwidth). The resulting probe distributions $f_n(\epsilon)$, not necessarily in the form of Fermi functions, are used in Eq. (7) to reach the net charge current.

Voltage Probe. Local inelastic-dissipative effects can be introduced into the wire by demanding that the net total particle current flowing between each probe and the system, Eq. (9), vanishes,

$$I_n = 0. \quad (15)$$

Out-of-equilibrium, these N equations can be solved numerically, as was done in phononic models[68]. Analytic results for μ_n can be reached in linear response[56],

$$\mu_n \sum_\alpha \int_{-\infty}^\infty \left(-\frac{\partial f_{eq}}{\partial \epsilon}\right) \mathcal{T}_{n,\alpha}(\epsilon) d\epsilon$$
$$-\mu_{n'} \sum_{n'} \int_{-\infty}^\infty \left(-\frac{\partial f_{eq}}{\partial \epsilon}\right) \mathcal{T}_{n,n'}(\epsilon) d\epsilon$$
$$= \int_{-\infty}^\infty d\epsilon \left(-\frac{\partial f_{eq}}{\partial \epsilon}\right) [\mathcal{T}_{n,L}(\epsilon)\mu_L + \mathcal{T}_{n,R}(\epsilon)\mu_R]. \quad (16)$$

We can further simplify Eq. (16) at low enough temperatures, $1/\beta < \gamma_\nu$. In this limit, the transmission function is assumed to be flat in the vicinity of the Fermi energy, in a region where the Fermi function suffers significant changes, $\frac{\partial f_{eq}(\epsilon)}{\partial \epsilon} \sim -\delta(\epsilon - \epsilon_F)$.

At low applied bias, the dephasing and voltage similarly operate. This can be justified by noting that in linear response and at low enough temperatures the voltage

probe can support energy exchange processes only within a small energy interval, $\mu_n - \mu_F$, thus it acts similarly to the dephasing probe (see Fig. 8).

What does a dephasing probe do? While in the local-site basis this probe enforces the condition of zero *energy resolved* flux between the every site and its local probe, upon transforming the Hamiltonian of the wire (2) from the site representation to the energy basis we find that the dephasing probe can drive transitions between molecular orbitals: We define the molecular eigenstates by the fermionic creation operator $\hat{d}_m^\dagger$, $\hat{H}_W = \sum_m E_m \hat{d}_m^\dagger \hat{d}_m$, then formally expand the local-site operators, $\hat{c}_n = \sum_m \lambda_{n,m} \hat{d}_m$. In the energy basis the N probes are coupled to the N molecular orbitals, $\hat{V}_P = \sum_{n,m} \lambda_{n,m} g_{n,k} \hat{a}_{n,k}^\dagger \hat{d}_m + h.c.$, providing a mechanism for (environmentally-mediated) transitions between molecular electronic states. The energy resolved current to the n probe is given by

$$I_{n,k} = i \langle \sum_m \left(g_{n,k}^* \lambda_{n,m}^* \hat{d}_m^\dagger \hat{a}_{n,k} - g_{n,k} \lambda_{n,m} \hat{a}_{n,k}^\dagger \hat{d}_m \right) \rangle \tag{17}$$

Since under the dephasing probe we demand that $I_{n,k} = 0$, this expression reveals that the n probe takes electrons of energy ϵ_k e.g. from the mth orbital and disperses them into the other orbitals. For example, If we consider a single probe and two molecular orbitals, m_1 and m_2, the dephasing probe condition translates to the conservation law $I_{m_1 \to probe}(\epsilon) = I_{probe \to m_2}(\epsilon)$, i.e., the net energy flow to the probe is zero, but it exchanges electrons between orbitals.

Below we refer to the hybridization energy γ_d (molecule-dephasing probes) as "dephasing strength". As explained above, $\gamma_d/\hbar$ does not correspond to a "pure dephasing" process. This situation is similar to that reached with the perturbative (system-bath weak coupling) Redfield equation[43]: Bath-assisted dynamics had been admitted to the model by adding dephasing operators, acting locally on different sites of the wire. In the energy basis of the molecule these local bath operators were responsible for bath-induced transitions between molecular orbitals[42]. Given the probe conditions, the current leaving the L contact is identical to the current reaching the R terminal, $I_L = -I_R$.

C. Structured environment

The interaction of electrons with molecular vibrations is explicitly described by the following model

$$\hat{H} = \hat{H}_W + \hat{H}_L + \hat{H}_R + \hat{H}_T + \hat{H}_{ph} + \hat{H}_{e-ph}. \tag{18}$$

The molecular wire and the electrodes are the same as in Eqs. (2)-(4). The bosonic (phonon) environment and its coupling to electrons is given by

$$\hat{H}_{ph} = \sum_{q,n} \omega_{q,n} \hat{b}_{q,n}^\dagger \hat{b}_{q,n},$$

$$\hat{H}_{e-ph} = \sum_{q,n} h_{q,n} (\hat{b}_{q,n}^\dagger + \hat{b}_{q,n}) \hat{c}_n^\dagger \hat{c}_n.$$

Here $\hat{b}_{q,n}^\dagger$ ($\hat{b}_{q,n}$) stands for a bosonic creation (annihilation) operator responsible for exciting a mode of frequency q, coupled to the electron number operator $\hat{c}_n^\dagger \hat{c}_n$. The environment and its coupling energies $h_{q,n}$ provide the "spectral density" function $J_n(\omega) = \sum_q |h_{q,n}|^2 \delta(\omega - \omega_{q,n})$, possibly comprising a broad (low frequency) contribution, as well as discrete high frequency vibrational modes. It was illustrated in many studies that structured environments support involved dynamics in the subsystem; essentially, the back action of the bath on the system drives "non-Markovian" dynamics[38].

To model such effects within the LBP technique we suggest to adopt energy-dependent probe relaxation rates, defined in Eq. (13). Specifically, we use below the Debye-Drude function

$$\gamma_d(\epsilon) = 2\tilde{\gamma}_d \frac{\Omega |\epsilon|}{\epsilon^2 + \Omega^2} \tag{19}$$

which reaches the maximum value $\tilde{\gamma}_d$ at the cutoff frequency, $\gamma_d(\epsilon = \Omega) = \tilde{\gamma}_d$. Electrons arriving at the nth electronic site with energy $|\epsilon| \lesssim \Omega$ are likely to exchange energy with the probe's degrees of freedom. In contrast, electrons will not scatter to the probe terminals if $|\epsilon| \gg \Omega$, and they will coherently cross the junction. This behavior corresponds to the expected effects of electron-phonon interactions. In Sec. IV F we examine the role of a finite Ω on the conductance.

III. TRANSPORT MECHANISMS

In this Section we summarize results for the electrical conductance of molecular wires in (i) the coherent limit when $\gamma_d = 0$, see Fig. 2(a), and (ii) assisted by the environment with $\gamma_d \neq 0$, see Fig. 2(b).

A. Coherent electrons: Ballistic motion and Tunneling

In the absence of the probes, $\gamma_d = 0$, the current obeys the standard Landauer expression,

$$I_L = \frac{e}{2\pi\hbar} \int_{-\infty}^{\infty} d\epsilon \mathcal{T}_{L,R}(\epsilon) [f_L(\epsilon) - f_R(\epsilon)]. \tag{20}$$

Pronounced temperature dependence of transport characteristics is typically attributed to the hopping mechanism, but the current can also strongly depend on temperature in coherent tunneling due to the Fermi functions in this expression. We illustrate this next. We consider the contribution of a single-dominant narrow resonance,

$$\mathcal{T}_{L,R}(\epsilon) \sim \gamma A(\epsilon_B) \delta(\epsilon - \epsilon_B). \tag{21}$$
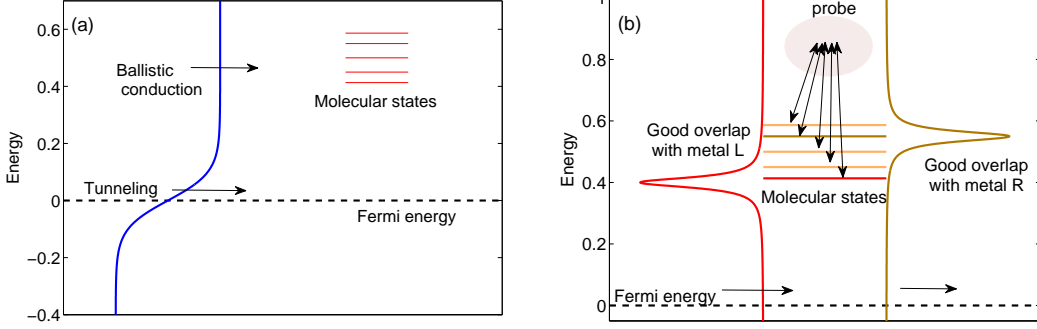
FIG. 2. Dominant transport mechanisms in the LBP molecular wire model. (a) Off-resonant tunneling and (resonant) ballistic conduction when $\gamma_d = 0$. The blue line at the left end describes the Fermi distribution function of incoming electrons. (b) Illustration of bath (probe) assisted transport, depicting for simplicity a single probe. While all molecular orbitals are broadened, we explicitly demonstrate the broadening of two orbitals, those that are strongly coupled to the left and right metals. Incoming electrons of energy ϵ, possibly at the tail of the broadening function, are scattered between the probes and the molecular states, then emitted to the R lead. Energy conservation is imposed by the dephasing probe.

Here A as a dimensionless prefactor. We highlight its dependence on the bridge energetics, but it may further depend on other molecular parameters, inter-site tunneling v, hybridization to the electrodes γ_ν and molecular length N. The prefactor γ, the harmonic average of γ_L and γ_R, has been included here as the resonance width. Using this narrow-resonance form, Eq. (20) reduces to

$$
\begin{aligned}
I_L &= \frac{e}{2\pi\hbar}\gamma A(\epsilon_B)[f_L(\epsilon_B) - f_R(\epsilon_B)] \\
&= \frac{e}{2\pi\hbar}\gamma A(\epsilon_B)e^{\beta\epsilon_B}[e^{-\beta\mu_R} - e^{-\beta\mu_L}]f_L(\epsilon_B)f_R(\epsilon_B).
\end{aligned}
\tag{22}
$$

In the linear response limit, $\beta\Delta\mu < 1$, we expand the functions to the lowest nontrivial order in voltage,

$$
\begin{aligned}
G &= G_0\gamma\beta A(\epsilon_B)\frac{e^{\beta\epsilon_B}}{(e^{\beta\epsilon_B} + 1)^2} \\
&\xrightarrow{\beta\epsilon_B \gg 1} G_0\beta\gamma A(\epsilon_B)e^{-\beta\epsilon_B}.
\end{aligned}
\tag{23}
$$

The combination $\beta e^{-\beta\epsilon_B}$ suppresses the tunneling conductance at both low and high temperatures, providing a temperature dependence distinctively different from standard Arrhenius behavior. Here $G_0 = e^2/2\pi\hbar$; we left out the factor of $\times 2$ coming from the spin degree of freedom.

Going back to Eq. (22), we now consider a finite bias situation, $\beta\Delta\mu > 1$. In this case we maintain only the larger factor $e^{\beta\Delta\mu}$ in the numerator of Eq. (22), for $\Delta\mu > 0$, and again take the limit $\beta\epsilon_B \gg 1$. We now reach an Arrhenius activation form for the conductance[26],

$$
G = G_0\gamma A(\epsilon_B)e^{-\beta(\epsilon_B - |e\Delta V|/2)}.
\tag{24}
$$

Eqs. (23)-(24) describe contribution to conductance from thermally excited electrons, populating energies in resonance with a narrow molecular orbital of energy ϵ_B. These electrons cross the molecule in a ballistic manner

as dephasing and inelastic terms are missing from these formulae.

Next, we broaden the resonance (21). This allows electrons at the Fermi energy to cross the bridge, off-resonance. We assume (i) that the applied bias is small to expand $f_\nu(\epsilon) \sim f_{eq}(\epsilon) - \frac{\partial f_{eq}}{\partial\epsilon}(\mu_\nu - \epsilon_F)$, and (ii) that the transmission function is almost flat (constant) close to the Fermi energy. We then reach the following, well-known, result

$$
\begin{aligned}
I_L &= \Delta\mu\frac{e}{2\pi\hbar}\mathcal{T}_{L,R}(\epsilon_F)\int_{-\infty}^{\infty}\frac{-\partial f_{eq}(\epsilon)}{\partial\epsilon}d\epsilon \\
&= \Delta\mu\frac{e}{2\pi\hbar}\mathcal{T}_{L,R}(\epsilon_F).
\end{aligned}
\tag{25}
$$

The conductance is proportional to the transmission evaluated at the Fermi energy, and it does not depend on temperature,

$$
G = G_0\mathcal{T}_{L,R}(\epsilon_F).
\tag{26}
$$

In the "deep tunneling" regime when the barrier height is large, $\epsilon_B > v, \gamma_\nu$, the transmission function can be simplified into the "superexchange" expression[5]

$$
\begin{aligned}
\mathcal{T}_{L,R}(\epsilon_F) &\approx \\
&\frac{\gamma_L\gamma_R v^2}{[(\epsilon_B - \epsilon_F)^2 + (\gamma_L/2)^2][(\epsilon_B - \epsilon_F)^2 + (\gamma_R/2)^2]} \\
&\times\left(\frac{v}{\epsilon_B - \epsilon_F}\right)^{2(N-2)} \\
&\xrightarrow{\epsilon_B \gg \gamma_\nu} \frac{\gamma_L\gamma_R}{v^2}\left(\frac{v}{\epsilon_B - \epsilon_F}\right)^{2N} \\
&= \left(\frac{\gamma_L\gamma_R}{v^2}\right)e^{-aN\left(\frac{2}{a}\ln\left|\frac{\epsilon_B - \epsilon_F}{v}\right|\right)}.
\end{aligned}
\tag{27}
$$

Recall that we set energies relative to the Fermi energy ($\epsilon_F = 0$). Eq. (27) indicates that the conductance decays exponentially with molecular size, $L \equiv aN$, with a as a

unit length. Identifying the tunneling decay constant by $\kappa \equiv \frac{2}{a} \ln |\frac{\epsilon_B}{v}|$ (often denoted by β in the literature, here reserved for the inverse temperature), we arrive at the familiar form

$$G \sim G_0 e^{-\kappa L}. \tag{28}$$

Fig. 2(a) depicts the ballistic [Eqs. (23)-(24)] and tunneling [Eq. (27)] contributions to the current.

B. Bath-assisted transport

Calculations based on perturbative master equation formalisms suggest that long-range electrical conduction may be captured by a rational function[43], corresponding to experimental observations of long-range ohmic-like conduction in molecular wires[9,10,12–15,18–22]. In Sec. IV we present detailed simulations using the LBP technique, and based on observations, we construct the following form for the hopping (H) conduction,

$$G_H \sim G_0 A(T) \frac{v^2}{\epsilon_B^4} \frac{\gamma_d^2}{N+l}. \tag{29}$$

It is valid when the bridge is high $\epsilon_B \gg v, \gamma_d, \Delta\mu$, as well as $\epsilon_B > \gamma$, and in the range $15 < \beta\epsilon_B < 30$. This corresponds to $\epsilon_B = 0.5$ eV and temperatures in the range ± 150 K around room temperature. As before, N stands for the number of repeating units in the wire, γ_d is the dephasing strength, v the intersite tunneling, ϵ_B the bridge energy relative to the Fermi energy, $A(T)$ a dimensionless prefactor which depends on temperature, possibly in a form weaker than the "bare" Arrhenius factor, e.g., $A(T) \sim \beta e^{-\beta E_A}$, with an activation energy E_A, linearly proportional to ϵ_B. The parameter l is introduced to accommodate the tunneling-to-hopping transition point, see for example Fig. 3.

Similarly to environmentally assisted DBA-ET rates, Eq. (29) describes an ohmic conduction, it depends on v^2, and as expected, grows with γ_d. However, an exact correspondence to ET rates is missing[41,42,44–47,72,73]. While these two quantities, DBA-ET rate and the electrical conductance (examined here) are obviously related, their properties are fundamentally different in some ways: DNA-ET processes involve electron localization on the donor and acceptor sites whereas in a molecular wire setup electrons are transferred through the bridge between metal electrodes. Thus, the hybridization energy of the bridge to the metals and the thermal occupation factor of electrons in the bulk largely determine the electrical conductance. Furthermore, in DBA situations the Franck-Condon factor, taking into account the energy difference between donor and acceptor states and the solvent-induced reorganization energy, dictates the transmission rate, while it is missing from molecular electronic conduction[75,76]. Theoretical studies have predicted a linear relationship between DBA-ET rates and the conductance (for molecules with high barriers), but experiments indicate that these two quantities are not simply linearly correlated[81], possibly due to differences in bath-induced decoherence rates and bridge energetics[71].

Fig. 2(b) schematically depicts the probe-assisted hopping conduction, Eq. (29). While in DBA-ET situations electrons can populate the bridge only if thermally excited, in the junction setup the molecular orbitals are broadened due to their hybridization to the metals [Lorentzian lineshapes in Fig 2(b)], and this broadening allows electron to occupy molecular states without thermal activation.

We further argue that at low temperatures, equation (29) should be generalized to

$$G_D = G_0 \sum_{m=2,3..}^{N} \left(\frac{v^{m-1}}{\epsilon_B^m} \right)^2 F_m(\gamma_L, \gamma_R, \gamma_d, T). \tag{30}$$

interpolating between the coherent result (27) using $F_N = \gamma_L \gamma_R$ and $F_{m<N} = 0$ and the hopping limit (29) when $F_2 \sim A(T)\gamma_d^2/(N+l) \gg F_{m>2}$.
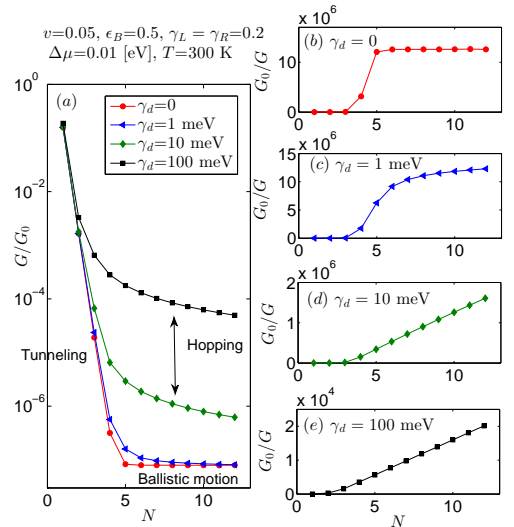
FIG. 3. Electrical conductance as a function of molecular length N at $T = 300$ K using different dephasing strengths, γ_d=0, 1, 10 and 100 meV, as indicated in the figure caption, (dephasing probe condition). (a) A semi-logarithmic plot demonstrates that G decays exponentially with length in short chains at weak dephasing. (b)-(e) An inverse algebraic behavior (29), $G^{-1} \propto N$, is established for long chains at large enough dephasing. Dominating transport mechanisms are marked in panel (a).

IV. RESULTS: TUNNELING TO HOPPING CONDUCTION

We describe here the LBP numerical simulations of molecular electronic conduction (mostly under the dephasing probe), with the goal to construct an approximate closed-form expression for the hopping conduction, as reported in Eq. (29). We focus on a uniform-
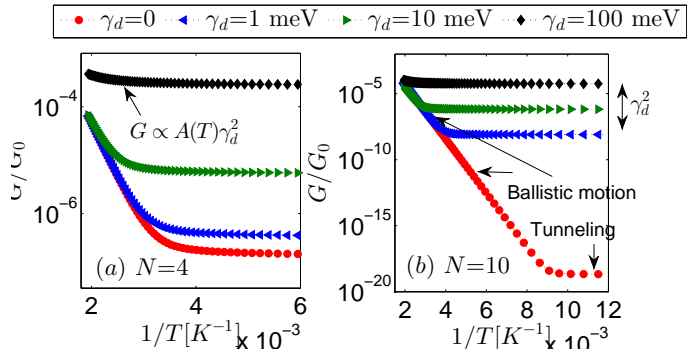
FIG. 4. Temperature dependence of the electrical conductance for (a) $N = 4$-site wire and (b) $N = 10$-site wire, demonstrating tunneling behavior at low temperatures, ballistic-resonant activated conduction at high temperatures, and hopping behavior when $\gamma_d \neq 0$, at low-intermediate temperatures. Parameters are $\epsilon_B = 0.5$, $v = 0.05$, and $\gamma_L = \gamma_R = 0.2$, $\Delta\mu = 0.001$ eV, dephasing probe condition.
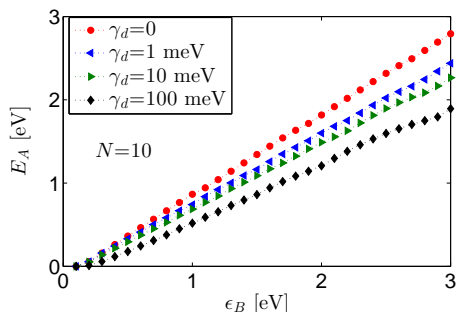

FIG. 5. Activation energy E_A, as resolved from Arrhenius plots as in Fig. 4, plotted against the bridge energy ϵ_B, demonstrating a linear relationship. Parameters are indicated in Fig. 4.

symmetric system, $\epsilon_B = \epsilon_n = 0.5 - 1$ eV, $v_{n,n\pm1} = v = 0.05 - 0.3$ eV and $\gamma_L = \gamma_R = 0.2 - 1$ eV. The temperature of the L and R leads, as well as the probes, is taken within the range $T = 150 - 400$ K, fixed across the junction. In this section we restrict simulations to the low voltage regime, $\Delta\mu = 10^{-4} - 0.01$ eV. The voltage shifts the position of the Fermi energy at the contacts, $\mu_L = \mu_F + e\Delta V/2$, $\mu_R = \mu_F - e\Delta V/2$, but bridge energies are intact. In Sec. V we study the role of a large applied voltage $\Delta\mu \sim 0.1 - 2$ eV on the transport behavior. The dephasing strength γ_d (probe hybridization) is taken uniform along the chain. We provide it in units of eV; when divided by $\hbar$ it translates to a rate constant.

The net current flowing under an applied bias $\Delta\mu$ is calculated in three steps: (i) We construct the matrices $\mathbf{G}$ and $\mathbf{\Gamma}_\alpha$, then the transmission coefficient between every two terminals $\mathcal{T}_{\alpha,\alpha'}(\epsilon)$ from Eq. (10). (ii) We include environmental effects e.g. with dephasing probes. This is achieved by calculating (numerically) the functions $f_n(\epsilon)$ using the probe condition (14). (iii) We evaluate the net-total current from the L electrode via Eq. (7). As

mentioned above, the probe conditions ensure that the current leaving the L metal is identical to the current arriving at the right electrode, $I \equiv I_L = -I_R$. For dephasing probe, moreover, $I(\epsilon) \equiv I_L(\epsilon) = -I_R(\epsilon)$.

A. Length dependence

The behavior of the conductance with increasing molecular length is displayed in Fig. 3 under a range of dephasing energies, $\gamma_d = 0 - 100$ meV. In the absence of dephasing the conductance decays exponentially with molecular length for $N \sim 1 - 5$, in agreement with Eq. (27), but beyond that it is fixed (and small), independent of size. This residual component emerges due to incoming electrons of energy ϵ_B (occupying the tail of the Fermi function), which are crossing the junction ballistically. In contrast, at finite dephasing strengths and beyond $N \sim 5$ the tunneling behavior is overpowered by a hopping-ohmic contribution $G^{-1} \propto N$. Fig. 3 establishes two central results for hopping conduction: at finite dephasing strength long-range electron transfer follows an ohmic form, and that $G \propto \gamma_d^2$ in this region.

B. Thermal activation

The onset of an Arrhenius behavior at high enough temperatures is considered a central characteristic of hopping dynamics in donor-bridge-acceptor electron transfer processes. However, Eq. (24) reveals that in metal-molecule-metal geometries a thermally activated conduction can take place even in the coherent regime, supporting ballistic-resonant behavior. In fact, electrons which are thermally activated in the metal are more likely to cross the junction ballistically rather than in an ohmic fashion (after being scattered between probes). Indeed we find that a clear Arrhenius dependency in our simulations corresponds to *ballistic* conduction, while a weaker temperature dependency may correspond to thermalized-yet-off-resonant electrons, hopping across the bridge.

Figure 4 displays this behavior. First, focus on the case of $\gamma_d = 0$ (red line). At very low temperatures the conductance does not depend on temperature at all (tunneling contribution). At high temperatures, an Arrhenius behavior is observed, with an activation energy E_A, indicating ballistic conduction at zero dephasing. Fig. 5 demonstrates that the activation energy E_A, the slope in the Arrhenius regime, $\log G \propto -\beta$, linearly follows the bridge height ϵ_B.

At finite dephasing strength the situation is rather involved. Let us first focus on the low temperature regime of Fig. 4. While the temperature dependence is rather weak, it is clear that G is increasing as $G \propto \gamma_d^2$. This indicates on an activation-less dephasing assisted conductance, see Eq. (29). At high temperatures and for long wires (see for example $N = 10$, $T^{-1} = 0.03$ K^{-1}) the conductance shows an activated form, but it does not depend

on γ_d, for $\gamma_d = 1-10$ meV. This again points to a ballistic motion; the dominant role of temperature is to enhance the population of electrons in resonance with the bridge, with the ballistic component dominating hopping contribution. Thermally-activated hopping conduction (29) further shows up, but only when the dephasing strength is high and the bridge is short, see $N = 4$, $T^{-1} = 0.02$ K^{-1} and $\gamma_d = 100$ meV.

To summarize, unlike DBA-ET rates, activated conductance in junctions does not expose transport mechanisms: At low temperatures, a seemingly activationless conductance may reflect either deep-tunneling or dephasing-assisted conduction of deep electrons. Similarly, activated transport at high temperatures may correspond to both ballistic and ohmic components.

C. Dephasing

The role of dephasing strength γ_d on the conductance is explored in Fig. 6, and we observe a characteristic "Kramers-like" turnover behavior[82]. At low dephasing the conductance increases with γ_d as it opens up a new route for electrons to cross the bridge, by hopping between sites. At large dephasing strengths $\gamma_d/\epsilon_B \gtrsim 2$ the conductance drops approximately as γ_d^{-1}. In a classical language one attributes this decay to the impediment of electrons at strong friction, resulting in an overdamped dynamics. This Kramers-like turnover behavior was demonstrated in other studies of electron transfer[41,42,46,47]. Investigations based on Redfield[42] and Lindblad equations[47] even provided a very similar value for the turnover point. Related trends were also observed in recent explorations of environmental-assisted quantum energy transport in light-harvesting biomolecules[83].

Note that in the Kramers' theory the barrier crossing rate first increases *linearly* with friction strength, then decreases as the inverse of friction. Here, we observe a more intricate behavior: The LBP conductance increases linearly with dephasing in short chains, $G \propto \gamma_d$, but in long chains the enhancement follows $G \propto \gamma_d^2$, in the weak-dephasing regime.

The quadratic dependence $G \propto \gamma_d^2$ is a direct result of the phenomenological-probe modelling of bath-assisted electron scatterings. Unlike a genuine electron-phonon scattering process, in which an electron is scattered *between* different electronic states assisted by a phonon, the probes *absorb* an electron and emit it (possibly) at a different molecular state, to be re-absorbed by another probe. This probe-molecule-probe transfer process of electrons results in the γ_d^2 functional form, in analogy with the $\gamma_L \times \gamma_R$ term in Eq. (27). In short chains, the L and R metals-to-probes scattering is significant, more than multiple probe-molecule-probe electron scattering, to construct the prefactor $\gamma\gamma_d$. While the quadratic dependence is not necessarily physical, it is yet encouraging to find that the Kramers-like turnover is well reproduced here, in a seemingly correct value.
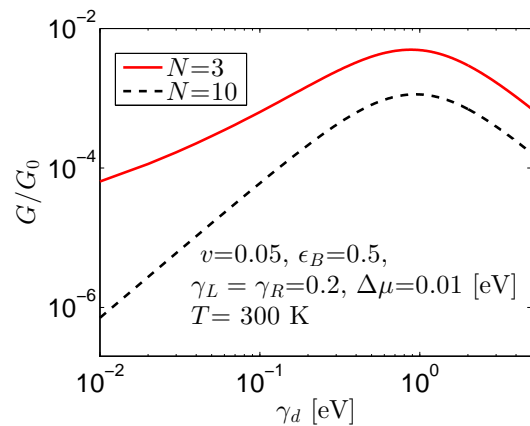

FIG. 6. Kramers-like behavior of the electrical conductance with dephasing strength (dephasing probe). Parameters are indicated within the figure.

D. Junction's energetics

To further expose the dependence of the hopping conductance on the junction's energy parameters, we study the behavior of G with ϵ_B (set relative to the Fermi energy), inter-site tunneling v, and the hybridization energy $\gamma_{L,R}$. As before, we restrict parameters to the regime $\epsilon_B > v, \gamma_{L,R}$.

In Fig. 7 we display the conductance as a function of ϵ_B for $N = 8$ and $N = 12$ under nonzero dephasing and reveal a crossover from $G \sim e^{-\beta\epsilon_B}$ to $G \sim \frac{1}{\epsilon_B^4}$, corresponding to the transition between a ballistic behavior (no length dependence) dominating at small ϵ_B, to off-resonance dephasing-induced hopping conduction.

We now analyze more carefully the dependence of the conductance on temperature and bridge energy. We recall that two limiting mechanisms prevail in the absence of dephasing effects: deep tunneling conduction and ballistic transmission. Ballistic motion dominates in long
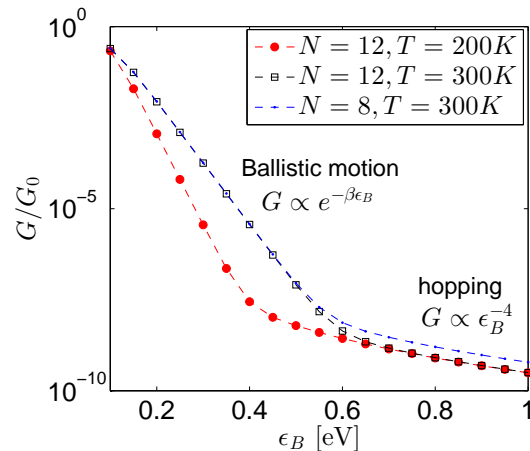

FIG. 7. Conductance as a function of the bridge energy ϵ_B. $v = 0.05$, $\gamma_{L,R} = 0.2$, $\gamma_d = 10^{-3}$ (dephasing probe) and $\Delta\mu = 0.01$ eV.
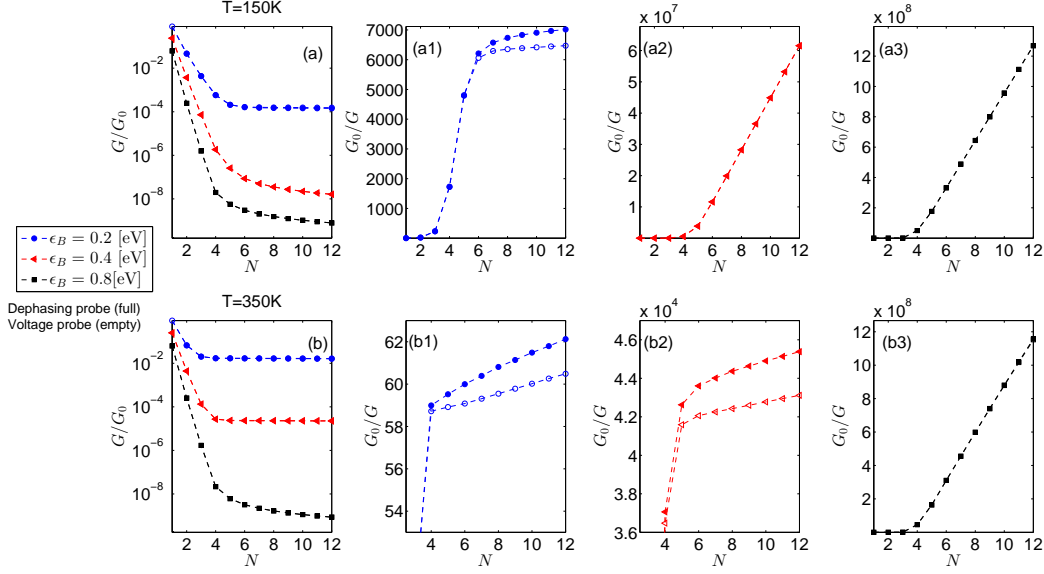
FIG. 8. Analysis of bath-assisted conduction, $\gamma_d = 1$ meV. (a) At low temperatures $T = 150$ K and for high bridges an activation-less transport takes place. (b) At high temperatures $T = 350$ K the conductance is enhanced by a thermal factor. Panels (a1)-(a4) and (b1)-(b4) expose the ohmic-like behavior in long wires, $v = 0.05$, $\gamma_{L,R} = 0.2$, $\Delta\mu = 0.01$ eV, dephasing probe condition (full symbols), voltage probe (empty symbols).

wires, and it carries the factor $\exp(-\beta\epsilon_B)$, see Eqs. (23)-(24), reflecting the thermal occupation of electrons in the metal at the bridge energy ϵ_B. Since it is non-dissipative, the ballistic component does not decay with distance, see Fig. 3. Dephasing-assisted conductance has a nontrivial temperature dependency due to the contribution of many electrons in the metal. In Fig. 8(a) we find that at low temperatures the conductance is missing an Arrhenius activation factor, $G(\epsilon_B = 0.4)/G(\epsilon_B = 0.8) \sim \left(\frac{0.8}{0.4}\right)^4 = 16$, while a different behavior takes place at high temperatures $T = 350$ K, as demonstrated in panel (b). Here, in conjunction with an ohmic-like decay, (focus on the red and black lines) $G(\epsilon_B = 0.4)/G(\epsilon_B = 0.8) \sim 10^5$, reflecting an activated-thermally enhanced conductance. We confirm in panels (b1)-(b3) that an ohmic-like behavior develops with $1/G \propto N$.

We also compare in Fig. 8 the operation of the dephasing and voltage probes. We find that at this low bias limit ($\Delta\mu = 10$ meV) transport characteristics are almost identical under either probes: the tunneling-to-hopping crossover takes place at a similar molecular bridge size, and the values for the conductances are close. The two probes show some deviations only when the bridge height is taken relatively low $\epsilon_B = 0.2$ eV, with the dephasing probe yielding lower values for conductance (larger resistance per site) in the hopping regime.

E. Hopping conduction: construction of Eq. (29).

Based on the simulations reported above, as well as additional results included in the Appendix, we suggest the hopping conductance, Eq. (29), $G_H \sim G_0 A(T) \frac{\gamma_d^2 v^2}{\epsilon_B^4} \frac{1}{N+l}$, with the dimensionless coefficient l, positive or negative, see Fig 7. This expression constitutes central characteristics of bath-assisted conduction: Ohmic-like conduction for long chains, and the enhancement of G with dephasing strength (for weak dephasing) and with barrier parameters as $\frac{v^2}{\epsilon^4}$. Recall that Eq. (29) was developed assuming parameters in the range $\gamma_d, v, \beta^{-1}, \Delta\mu \ll \epsilon_B$, $\gamma < \epsilon_B$,

We can justify this hopping form with some qualitative arguments: Electrons scatter into the molecule through the resonance most strongly hybridized with the L metal, and leave from the orbital most tightly coupled to the R lead, overall contributing the factor $\frac{v^2}{\epsilon^4}$. On the molecule, the probes absorb and emit electrons, dispersing them between molecular orbitals, thus the conductance scales as γ_d^2, describing probe-molecule-probe transitions. The contribution of probe-mediated scattering processes linearly grows with the number of molecular sites (probes), thus the hopping resistance grows as N. The overall temperature dependence in the process is rather weak; the hopping conductance integrates electrons thermally populating many levels in the lead, off-resonant as well as in resonance with molecular orbitals.

Both dephasing and voltage probes disperse electrons between molecular orbitals. However, the dephasing

probe does so while maintaining the number of electrons within each energy interval fixed. The voltage probe can absorb/provide energy from/to electrons, and it can thus modify the energy distribution of electrons in the system. At low bias, $\Delta\mu < \gamma_\nu, \beta^{-1}$, the two probes produce very similar conductance characteristics.

F.   Non-Markovian environment

We implement a structured environment by using energy-dependent dephasing energies with the Debye-Drude form, Eq. (19), see Fig. 9. As expected, we find that the conductance in the hopping regime is reduced due to the non-Markovianity of the bath, while the tunneling and ballistic regimes are unaffected. The effect is clearly observed at low temperatures, but it is significantly mitigated at higher temperatures, when the dominant mechanism is ballistic conduction.
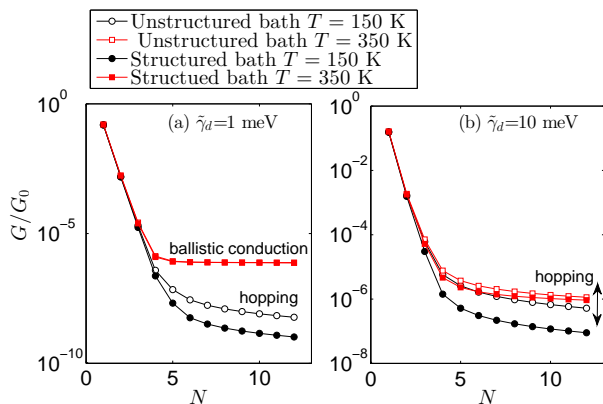

FIG. 9. Electrical conductance as a function of length using structured [Debye-Drude form, Eq. (19)] and unstructured (γ_d is a constant) environments at high and low temperatures. At low temperatures the conductance is sensitive to the cutoff frequency $\Omega = 0.1$ eV. We used $v = 0.05$, $\epsilon_B = 0.5$, $\gamma_{L,R} = 0.2$, $\Delta\mu = 0.01$ eV and $\tilde{\gamma}_d = 1, 10$ meV as indicated, dephasing probe condition. For unstructured environments we used $\gamma_d = 1, 10$ meV, independent of energy.

V.   BEYOND LINEAR RESPONSE: CURRENT-VOLTAGE CHARACTERISTICS

As a further application of our method, we present in Fig. 10 $I - V$ traces of molecular wires of size $N = 7$. These simulations were performed using the dephasing probe condition since the present implementation of the voltage probe is applicable only in the linear response regime. The voltage probe technique can be extended beyond that, by solving sets of nonlinear equations, see e.g. Ref.[80].

Considering molecules under a large applied bias, we need to first determine the details of the electrostatic potential profile across the junction. As was discussed

in several works[84–87], in the weak metal-molecule coupling limit the applied voltage typically drops only at the metal-molecule contacts (symmetrically or asymmetrically), thus the barrier maintains its equilibrium form. In contrast, at intermediate-strong molecule-metal coupling the applied bias largely drops across the molecule. Assuming a linear drop, the molecular barrier transforms from a rectangular to a trapezoidal shape, then to a triangular form when the bias exceeds the barrier height. This transition from a "direct tunneling" to "field emission transport" (Fowler-Nordheim tunneling) was explored experimentally with transition voltage spectroscopy (TVS), when plotting $\log(I/V^2)$ as a function of $1/V$ to extract the barrier height from the minima of this plot.

Here, we assume a linear potential profile and shift the energies of sites $n = 1, 2, ..., N$ accordingly,

$$\epsilon_n = \epsilon_B + \frac{\Delta\mu}{2} - \frac{\Delta\mu(n-1)}{N-1}. \tag{31}$$

Using this model, $I - V$ characteristics at different values for the dephasing strength are plotted in Fig. 10, as well as examples for the potential profile at low, intermediate, and large biases, see inset. The $I - V$ curves reveal the followings: Up to approximately 0.1 V a linear response behavior is maintained. The current is strongly enhanced when the voltage bias approaches a molecular resonance (located at ~ 0.5 eV). Beyond that, $\Delta\mu \gtrsim 2\epsilon_B$, the current saturates. The effect of the thermal bath on the $I - V$ characteristics is substantial. At low bias, dephasing effects assist electron conduction, $G \propto \gamma_d^2$. Further, in resonant situations while the current is saturated for $\gamma_d = 0$, it displays a negative differential conductance under dephasing. At large bias, the effect of dephasing on current is non-monotonic and deserves further attention.

We point that a detailed TVS analysis, or the application of similar[88] or alternative[89] measures, are not particularly illuminating here since we had adjusted the barrier, from a rectangular to a triangular shape, by hand, imposing the model (31). A TVS analysis or related investigations are interesting for e.g., exposing the evolution of the barrier height with size and contact properties in different families of molecules, such as alkanethiols chains or aromatic thiols systems[87].

VI.   COMPARISON TO EXPERIMENTS: ONI WIRES

In this Section we examine experimental results using the LBP method, to demonstrate the utility of the technique. Ref.[20] reported the resistance and current-voltage characteristics of conjugated oligonaphthalenefluoreneimine (ONI) molecular wires of different lengths, up to 10 nm with 10 repeating units, measured using conducting-probe atomic force (CP-AFM) microscopy. Based on the length-dependent and temperature-dependent resistance behavior, it was argued that short wires conduct via a coherent-tunneling
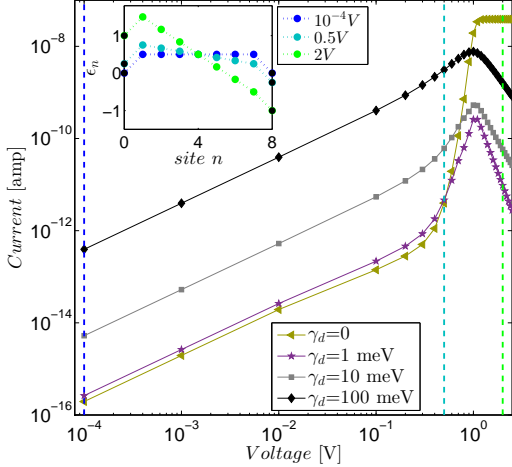
FIG. 10. $I - V$ traces for a molecular bridge seven units long with $T = 298$ K, $v = 0.05$, and $\gamma_{L,R} = 0.2$ eV. The bridge energies shift with the applied bias in a linear manner, Eq. (31), see examples in the inset. Sites $n = 0$ and $n = 8$ correspond to the chemical potentials at the contacts, μ_L and μ_R, respectively.

transport mechanism, while around 4 nm a transition in transport behavior, from tunneling to thermally-activated hopping, took place. Below, we use the data reported in Ref.[20] and extract relevant parameters for our model. We then demonstrate in Figs. 11-12 that by tweaking the dephasing rate and the temperature we can reasonably reproduce experimental results of transport in ONI wires, further providing some insights.

It should be emphasized that values for resistance reported in Ref.[20] correspond to a monolayer with $M \sim 100$; M is an estimate for the number of molecules under the measuring tip[20]. If we assume a linear scaling of the conductance, $G(M) \sim MG(1)$, the resistance should obey $R(M) \sim M^{-1}R(1)$. Certainly, this is an approximation which is not always justified; the conductance of a single-isolated wire $G(1)$ may significantly deviate from the monolayer conductance scaled-down, $G(M)/M$, due to cooperative effects, inter-wire couplings and substrate-mediated coupling. These effects may increase or decrease the conductance per wire[90–94]. A careful study of such effects with the LBP method is of interest. Here instead we use a naive-linear scaling approximation: We take resistance values reported in Figs. 6 and 8 of Ref.[20] and multiply them by $M = 100$; see the symbols $(+)$ in Figs. 11 and 12. Below we explain which parameters in our modelling are affected by this simplified scaling, and if so, the impact on analysis.

To uncover model parameters from Ref.[20], ϵ_B, v, $\gamma_{L,R}$, and γ_d, we first determine the unit length of the ONI wires to be $a \sim 1$ nm. We then obtain our parameters by following three steps:

(a) *Bridge energetics.* In the tunneling regime $N = 1 - 3$, $G \sim e^{-\kappa Na}$, with $\kappa = 2.5$ nm^{-1}[20]. Using the relation $\kappa \equiv \frac{2}{a} \ln |\frac{\epsilon_B}{v}|$ [see Eq. (27)], we resolve the ratio

$\epsilon_B/v = 3.4$. To obtain the bridge height ϵ_B and inter-site energies, separately, we note that the activation energy in ONI wires was approximated by $E_A \sim 0.55$ eV from an Arrhenius plot[20]. Furthermore, in Fig. 4 we found that while the activation energy linearly follows the bridge height, the slope deviates from unity, $\epsilon_B \sim 1.4E_A$ for $\gamma_d \sim 5$ meV. We thus select the value $\epsilon_B = 0.8$ eV, and immediately receive $v = 0.22$ eV. Note that these estimates are not affected by the scaling employed. Note also that the ballistic conductance is very sensitive to temperature near room temperature, and therefore is also very sensitive to the bridge height/activation energy. Even when using our "corrected" $\epsilon_B = 0.8$ value for bridge energy, we still observe excess ballistic conductance near room temperature, and can thus only match experimental results at a lower, "effective temperature".

(b) *Hybridization energy.* We resolve $\gamma_{L,R}$ from Eqs. (26)-(27) (using $G_0 = e^2/\pi\hbar$ to accommodate spin degree of freedom). We assume that this contact energy is identical at the two interfaces, and employ $\gamma_\nu = \sqrt{G/G_0} \times e^{\kappa Na}$. From the measured exponent $\kappa = 2.5$ nm^{-1} we receive $\gamma_\nu \sim 0.018$ eV. This estimate will vary if we adjust the scaling for $G(M)$, see discussion below.

(c) *Dephasing strength.* We approach this parameter, characterizing electron-vibration interaction in the molecule, by testing different values (uniform along the wire) in the range $\gamma_d = 0 - 100$ meV. In Fig. 11 we show that very small dephasing values $\gamma_d = 0 - 0.2$ meV reasonably reproduce both the exponent in the tunneling regime and the slope in the hopping-ohmic domain, assuming the junction's temperature is in the range 280-300 K. As mentioned above, a very good agreement is reached by slightly reducing the temperature; alternatively, higher bridge heights could be tested.

With these molecular parameters, we turn now to the Arrhenius plot of ONI wires, as reported in Ref.[20]. Figure 12 depicts $(+)$ the resistance as a function of inverse temperature for an $N = 7$ ONI wire, taken from Ref.[20], again linearly scaled down to the single molecule value. We find that our results agree fairly well with experimental data under a coherent transport mechanism, and we resolve the activation energy $E_A \sim 0.4$ eV from simulations, compared to the experimental value $E_A \sim 0.5$ eV. We try to reproduce this data using the parameters resolved in the discussion above, but find out that while at room temperatures and above, the experimental data is reasonably captured by our simulations with $\gamma_d \sim 3 - 4$ meV, at lower temperatures the experiment is reproduced with $\gamma_d = 0$ meV. A possible explanation for this behavior is that the dephasing rate in fact depends on temperature, $\gamma_d(T)$, and its value should be taken small $\gamma_d \ll 1$ meV at low temperatures, $T = 240$ K, while at room temperature it reaches values identified above.

Our analysis is based on the linear scaling assumption. It was demonstrated in Ref.[90] that this holds only beyond a certain molecular-island size of a few tens of molecules. Scaling the experimental results of Ref.[20] by $M \neq 100$

would alter our estimate for γ_ν and γ_d; recall that $G \propto \gamma_L \gamma_R$ in the tunneling regime and $G \propto \gamma_d^2$ in the hopping limit, see Sec. IV. As a limiting case, if reported values in Ref.[20] were to correspond to a single molecule rather than to $M \sim 100$ molecules, our simulations would fit the data with the same values for the bridge energetics, $\epsilon_B = 0.8$ eV, $v = 0.22$, but with (factor of 10 larger) $\gamma_L = \gamma_R = 0.18$ eV and $\gamma_d \sim 2$ meV. These values should serve as an upper estimate for dephasing strength.

Concluding our observations, the probe technique under weak dephasing as a tweaking parameter can capture the turnover behavior between superexchange and hopping regimes in molecular wires, given the correct system parameters as inputs. We also see from Fig. 11(a2), as well as in Fig. 12, that in order to match the experiment across all temperatures and lengths, the tuning parameter γ_d must depend on temperature, and that one should take into account corrections to the bridge height as it relates to the activation energy.
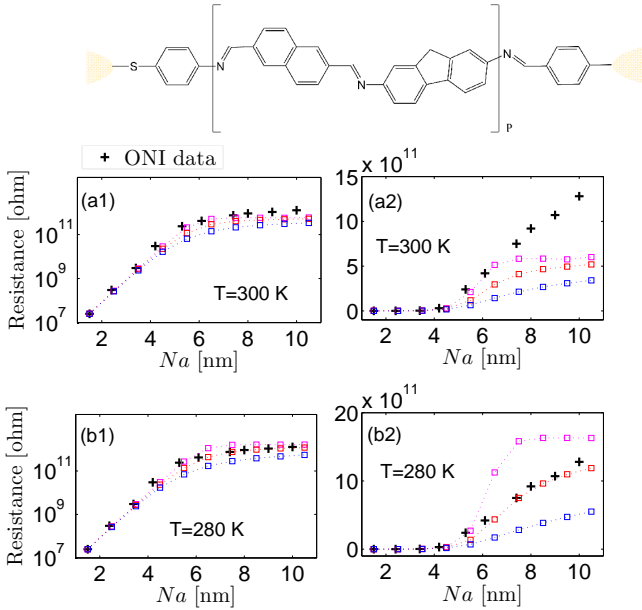

FIG. 11. Analysis of experimental results. We extracted data for the resistance of an ONI monolayer with $M \sim 100$ from Fig. 6 of Ref.[20], and multiplied it by $M = 100$ to approximate resistance per molecule. Top: a single ONI wire (length denoted by P here, rather than N, to eliminate confusion). (a)-(b) Experimental data $(+)$[20] as a function of molecular length, compared to probe-method simulations with $\gamma_d = 0, 0.2, 0.5$ meV, top to bottom (dotted lines with empty squares) assuming (a1)-(a2) $T = 300$ K and (b1)-(b2) $T = 280$ K. Panels (a1)-(b1) illustrate the tunneling region for $N = 1-4$, panels (a2)-(b2) uncover the ohmic behavior for $N > 5$. Dephasing-probe simulations were performed with $\epsilon_B = 0.8$ eV, $v = 0.22$ eV, $\gamma_{L,R}=0.018$ eV, applied voltage $\Delta\mu = 0.01$ eV and dephasing strengths in the range $\gamma_d = 0-1$ meV.
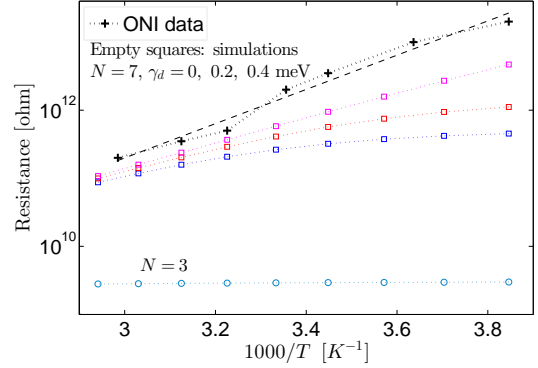

FIG. 12. Analysis of experimental results for the temperature dependence of conductance in ONI wires. Experimental data $(+)$[20] for $N = 7$ is compared to simulations with γ_d=0, 0.2, 0.4 meV (empty squares, top to bottom). For reference, we also show the $N = 3$ case $(\circ)$ in which the resistance is independent of dephasing in the range $\gamma_d \sim 0-5$ meV (consistent with the experiment). Other parameters are the same as in Fig. 11.

VII. CONCLUSIONS

We demonstrated that the Landauer-Büttiker probe technique can be used to simulate electronic conduction in molecular junctions under the influence of a thermal environment. The LBP approach can be incorporated with little effort into the commonly used Landauer-NEGF approach, to phenomenologically introduce bath-assisted site-to-site hopping conduction.

Our simulations revealed different transport mechanisms: In the absence of dephasing effects we identified deep-tunneling conduction in short wires and ballistic transport at high temperatures, a result of resonant transmission. Under finite dephasing strengths, hopping conduction was the dominant transport mechanism in wires of $N > 4$, showing temperature dependence which was generally weaker than the Arrhenius activation factor in the explored range of parameters.

Principal observations are: (i) Length-dependence investigations of molecular conduction immediately pinpoint the tunneling-to ohmic turnover. In contrast, activated conduction (or more generally, temperature dependent conduction) may show up in both the coherent (ballistic) and incoherent-hopping regimes. (ii) Kramers-like turnover behavior manifests itself under the LBP method. Weak dephasing effects promote hopping conduction, but dephasing becomes detrimental to transport when $\gamma_d \gtrsim \epsilon_B$. (iii) Structured environments can be implemented within the LBP method, by using energy-dependent dephasing coefficients. (iv) At large voltage biases, dephasing effects realize a negative differential conductance; this behavior is missing in the coherent limit. (v) A closed-form expression for the hopping conduction was constructed, Eq. (29), within stated parameters. (vi) The LBP method provided a semi-quantitative match for length dependent resistance in ONI wires re-

producing the tunneling to hopping crossover, as well as the resistance's temperature dependence- as long as we allow the dephasing strength to become temperature dependent.

Büttiker's probes offer an easily implemented mean to introduce dephasing and inelastic effects into molecular electronic applications, yet, obviously they do not absolutely correctly emulate physical process e.g., electron-vibration interaction. While overall the LBP approach ensures the conservation of current across the molecule, even within a small energy interval (dephasing probe), one should remember that the probes are metal electrodes, collection of Fermi sea electrons which themselves participate in the transport process. Essentially, the quadratic dependence of the hopping conductance on the probe hybridization ($G_H \propto \gamma_d^2$) reflects probe-molecule-probe electron scatterings, with an incoming electron from probe n arriving at the molecule, leaving it to probe n'; complementary processes ensure conservation of charge and energy, as necessary. In contrast, microscopic modelling of electron-vibration interactions should yield to lowest order a hopping conductance linear in the dephasing rate, possibly modifying Eq. (29), $\gamma_d^2 \to \gamma_d/\beta$. Thus, while the probes reproduce the hopping-ohmic nature of bath-assisted conduction, the predicted dephasing and temperature dependence should be taken with caution. To understand the correspondence of LBP results with physical-microscopic modelling, one should compare our simulations to projection-operator approaches and first-principle techniques[36].

In future studies we will examine the suitability of the LBP technique to describe the phenomenology of electronic function under environmental effects, e.g. consider molecular thermoelectricity under thermal effects[52,95] and the development of a diode behavior in symmetric molecules, induced by the surroundings[96].

ACKNOWLEDGMENTS

APPENDIX A: SUPPORTING SIMULATIONS FOR HOPPING CONDUCTANCE.

In the main text we established Eq. (29) by exploring the dependence of the hopping conductance on ϵ_B, γ_d, temperature and length. Here we complement this and examine the role of inter-site tunneling v and metal-molecule hybridization on G_H. In Fig. 13 we confirm that in the coherent-tunneling regime $G \propto v^{2N-2}$, but at finite dephasing and for large N we obtain $G \propto v^2$ for $v \ll \epsilon_B$, independent of molecular length (not shown).
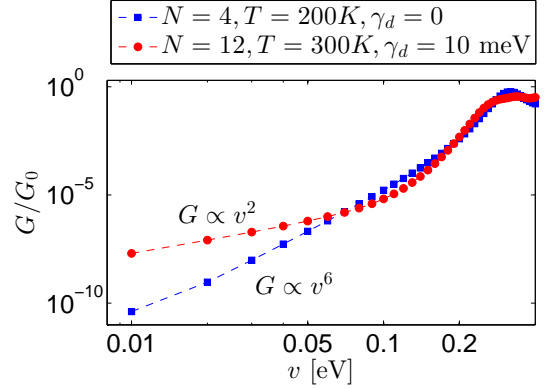

FIG. 13. Electrical conductance vs. inter-site tunneling v. In the coherent tunneling limit $G \propto \frac{1}{v^2}\left(\frac{v}{\epsilon_B}\right)^{2N}$. In the hopping regime $G \propto v^2$. Parameters used are $\epsilon_B = 0.5$, $v = 0.05$, $\gamma_\nu = 0.2$, $\Delta\mu = 0.01$ eV.
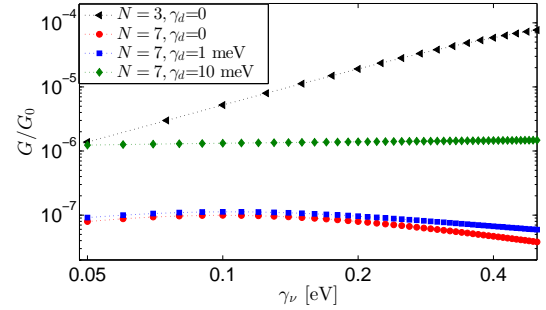

FIG. 14. Electrical conductance as a function of the hybridization energy, $\gamma_L = \gamma_R$. When $\gamma_d = 0$ we resolve tunneling conductance for $N = 3$, $G \propto \gamma_L \gamma_R$ ($\triangle$) and ballistic motion for $N = 7$ when $\gamma_\nu \ll \epsilon_B$ ($\circ$). The conductance dependency on γ_ν diminishes upon increasing dephasing strength. We used $T = 300$ K, $\epsilon_B = 0.5$, $v = 0.05$, $\Delta\mu = 0.01$ eV, dephasing probe simulations.

The hybridization energy γ_ν is expected to only mildly influence hopping conduction, as the resistance should be determined by the wire itself - electron scattering between probes- rather than by the interface of the molecule with the contacts. This behavior is confirmed in Fig. 14: Tunneling conductance ($N = 3$, $\gamma_d = 0$) grows as $\gamma_L \gamma_R$, see Eq. (27), but in long chains with $\gamma_d \neq 0$ the effect of the hybridization energy on G is insignificant.

[1] S. O. Kelley, and J. K. Barton, Science **283**, 375 (1999).
[2] N. B. Muren, E. D. Olmon, and J. Q. Barton, Phys. Chem. Chem. Phys. **14**, 13754 (2012).
[3] A. M. Kuznetsov, *Charge Transfer in Physics, Chemistry and Biology,* (Gordon and Breach, New York, 1995).
[4] V. May and O. Kuhn, *Charge and Energy Transfer Dynamics in Molecular Systems,* (WileyVCH, Berlin, 1999).
[5] A. Nitzan, *Chemical Dynamics in Condensed Phases: Relaxation, Transfer, and Reactions in Condensed Molecular Systems,* (Oxford University Press, Oxford, 2006).

[6] S. Datta, *Electronic Transport in Mesoscopic Systems*, (Cambridge University Press, New York, NY, 1995).

[7] J. C. Cuevas, *Scheer, E. Molecular Electronics: An Introduction to Theory and Experiment*, (World Scientific Publishing Company, Singapore, 2010).

[8] M. Di Ventra, *Electrical Transport in Nanoscale Systems*, (Cambridge University Press, Cambridge, U.K., 2008).

[9] F. D. Lewis, T. Wu, Y. Zhang, R. L. Letsinger, S. R. Greenfield, and M. R. Wasielewski, Science **277**, 673 (1997).

[10] B. Giese, Annu. Rev. Biochem. **71**(1), 51 (2002).

[11] J. C. Genereux, S. M. Wuerth, and J. K. Barton, J. Am. Chem. Soc. **133**(11), 3863 (2011).

[12] G. I. Livshits, A. Stern, D. Rotem, N. Borovok, G. Eidelshtein, A. Migliore, E. Penzo, S. J. Wind, R. Di Felice, S. S. Skourtis, J. C. Cuevas, L. Gurevich, A. B. Kotlyar, and D. Porath, Nat. Nanotech. **9**, 1040 (2014).

[13] Y. Selzer, M. A. Cabassi, T. S. Mayer, and D. L. Allara, Nanotechnology **15**, S483 (2004).

[14] Y. Selzer, M. A. Cabassi, T. S. Mayer, and D. L. Allara, J. Am. Chem. Soc. **126**, 4052 (2004).

[15] Y. Selzer, and D. L. Allara, Annu. Rev. Phys. Chem. **57**, 593 (2006).

[16] E. A. Weiss, M. J. Tauber, R. F. Kelley, M. J. Ahrens, M. A. Ratner, and M. R. Wasielewski, J. Am. Chem. Soc. **127**, 11842 (2005).

[17] R. H. Goldsmith, O. DeLeon, T. M. Wilson, D. Finkelstein-Shapiro, M. A. Ratner, and M. R. Wasielewski, J. Phys. Chem. A **112**, 4410 (2008).

[18] S. H. Choi, B. Kim, and C. D. Frisbie, Science **320**, 1482 (2008).

[19] L. Luo and C. D. Frisbie, J. Am. Chem. Soc. **132**, 8854 (2010).

[20] S. H. Choi, C. Risko, M. C. R. Delgado, B. Kim, J.-L. Bredas, and C. D. Frisbie, J. Am. Chem. Soc. **132**, 4358 (2010).

[21] L. Luo, S. H. Choi, and C. D. Frisbie, Chem. Mater. **23**, 631 (2011).

[22] L. Luo, A. Benameur, P. Brignou, S. H. Choi, S. Rigaut, and C. D. Frisbie, J. Phys. Chem. C **115**, 19955 (2011).

[23] Q. Lu, ; K. Liu, H. Zhang, Z. Du, X. Wang, and F. Wang, ACS Nano **12**, 3861 (2009).

[24] S. A. Di Benedetto, A. Facchetti, M. A. Ratner, and T. J. Marks, J. Am. Chem. Soc. **131**(20), 7158 (2009).

[25] T. Hines, I. Diez-Perez, J. Hihath, H. Liu, Z. S. Wang, J. Zhao, G. Zhou, K. Müllen, and N. Tao, J. Am. Chem. Soc. **132**, 11658 (2010).

[26] G. Sedghi, V. M. Garcia-Suarez, L. J. Esdaile, H. L. Anderson, C. J. Lambert, S. Martin, D. Bethell, S. J. Higgins, M. Elliott, N. Bennett, J. E. Macdonald, and R. J. Nichols, Nature Nanotech. **6**, 517 (2011).

[27] Z. Li, T.-H. Park, J. Rawson, M. J. Therien, and E. Borguet, Nano Lett. **12**, 2722 (2012).

[28] S. K. Lee, R. Yamada, S. Tanaka, G. S. Chang, Y. Asai, and H. Tada, ACS Nano **6**, 5078 (2012).

[29] L. Sepunaru, N. Friedman, I. Pecht, M. Sheves, and D. Cahen, J. Am. Chem. Soc. **134**, 4169 (2012).

[30] V. Kaliginedi, A. V. Rudnev, P. Moreno-Garcia, M. Baghernejad, C. Huang, W. Hong, and T. Wandlowski, Phys. Chem. Chem. Phys. **16**, 23529 (2014).

[31] C. C. Bof Bufon, C. Vervacke, D. J. Thurmer, M. Fronk, G. Salvan, S. Lindner, M. Knupfer, D. R. T. Zahn, and O. G. Schmidt, J. Phys. Chem. C **118**, 7272 (2014).

[32] A. Mitra, I. Aleiner, and A. J. Millis, Phys. Rev. B **69**, 245302 (2004).

[33] F. Haupt, M. Leijnse, H. L. Calvo, L. Classen, J. Splettstoesser, and M. R. Wegewijs, Physica Status Solidi B **250**, 2315 (2013).

[34] M. Galperin, M. A. Ratner, and A. Nitzan, J. Phys.: Condens. Matter **19**, 103201 (2007).

[35] R. Hützen, S. Weiss, M. Thorwart, and R. Egger, Phys. Rev. B **85**, 121408 (2012).

[36] L. Simine and D. Segal, J. Chem. Phys. **138**, 214111 (2013).

[37] E. Y. Wilner, H. Wang, M. Thoss, and E. Rabani, Phys. Rev. B **89**, 205129 (2014).

[38] H. P. Breuer and F. Petruccione, Oxford University Press, Oxford, (2002).

[39] A. K. Felts, W. T. Pollard, and R. A. Friesner, J. Phys. Chem. **99**, 2929 (1999).

[40] A. Okada, V. Chernyak, and S. Mukamel, J. Phys. Chem. A **102**, 1241 (1998).

[41] W. B. Davis, M. R. Wasielewski, M. A. Ratner, V. Mujica, and A. Nitzan, J. Phys. Chem. A **101**, 6158 (1997).

[42] D. Segal, A. Nitzan, W. B. Davis, M. R. Wasielewsky, and M. A. Ratner, J. Phys. Chem. B **104**, 3817 (2000).

[43] D. Segal, A. Nitzan, M. A. Ratner, and W. B. Davis, J. Phys. Chem. B **104**, 2790 (2000).

[44] E. G. Petrov, Ye. V. Shevchenko, V. I. Teslenko, and V. May, J. Chem. Phys. **115**, 7107 (2001).

[45] E. G. Petrov and V. May, J. Phys. Chem. A **105**, 10176 (2001).

[46] E. A. Weiss, G. Katz, R. H. Goldsmith, M. R. Wasielewski, M. A. Ratner, R. Kosloff, and A. Nitzan, J. Chem. Phys. **124**, 074501 (2006).

[47] M. Zarea, D. Powell, N. Renaud, M. R. Wasielewski, and M. A. Ratner, J. Phys. Chem. B **117**(4), 1010 (2013).

[48] N. Renaud, Y. A. Berlin, F. D. Lewis, and M. A. Ratner, J. Am. Chem. Soc. **135**, 3953 (2013).

[49] U. Harbola, M. Esposito, and S. Mukamel, Phys. Rev. B **74**, 235309 (2006).

[50] C. Timm, Phys. Rev. B **77**, 195416 (2008).

[51] L. Kecke and J. Ankerhold, arXiv:1301.2422.

[52] D. Segal, Phys. Rev. B **72**, 165426 (2005).

[53] L.-Y. Hsu, N. Wu, and H. Rabitz, J. Phys. Chem. Lett. **5**, 1831 (2014).

[54] M. Büttiker, Phys. Rev. B **33**, 3020 (1986).

[55] J. Damato and H. M. Pastawski, Phys. Rev. B **41**, 7411 (1990).

[56] D. Roy and A. Dhar, Phys. Rev. B **75**, 195110 (2007).

[57] J. H. Jiang, O. Entin-Wohlman, and Y. Imry, Phys. Rev. B **85**, 075412 (2012).

[58] G. Benenti, K. Saito, and G. Casati, Phys. Rev. Lett. **106**, 230602 (2011).

[59] S. Bedkihal, M. Bandyopadhyay, and D. Segal, Euro. Phys. J. B **86**, 506 (2013).

[60] Y. Utsumi, O. Entin-Wohlman, A. Aharony, T. Kubo, and Y. Tokura, Phys. Rev. B **89**, 205314 (2014).

[61] Y. Xue, S. Datta, and M. Ratner, Chem. Phys. **281**, 151-170 (2002).

[62] W. M. Visscher and M. Rich, Phys. Rev. A **12**, 675 (1975).

[63] F. Bonetto, J. L. Lebowitz, and J. Lukkarinen, J. Stat. Phys. **116**, 783 (2004).

[64] A. Dhar and D. Roy, J. Stat. Phys. **125**, 801 (2006).

[65] D. Roy, Phys. Rev. E **77**, 062102 (2008).

[66] D. Segal, Phys. Rev. E **79**, 012103 (2009).

[67] F. Barros, H. C. F. Lemos, and E. Pereira, Phys. Rev. E **74**, 052102 (2006).

[68] M. Bandyopadhyay and D. Segal, Phys. Rev. E **84**, 011151 (2011).

[69] K. Saaskilahti, J. Oksanen, and J. Tulkki, Phys. Rev. E **88**, 012128 (2013).

[70] S. G. Chen, Y. Zhang, S. K. Koo, H. Tian, C. Y. Yam, G. H. Chen, and M. A. Ratner, J. Phys. Chem. Lett. **5**, 2748 (2014).

[71] R. Venkataramani, E. Wierzbinski, D. H. Waldeck, and D. N. Beratan, Farady Disucssion **174**, 57 (2014).

[72] D. N. Beratan, C. Liu, A. Migliore, N. F. Polizzi, S. S. Skourtis, P. Zhang, and Y. Zhang, Acc. Chem. Res., **48**, 474 (2014).

[73] A. Troisi, M. A. Ratner, and A. Nitzan, J. Chem. Phys. **119**, 5782 (2003).

[74] J. Lehmann, G.-L. Ingold, and P. Hänggi, Chemical Physics **291**, 199 (2002).

[75] A. Nitzan, J. Phys. Chem. A **105**(12), 2677 (2001).

[76] A. Nitzan, Isr. J. Chem. **42**, 163 (2002).

[77] P. Reddy, S.-Y. Jang, R. A. Segalman, and A. Majumdar, Science **315**, 1568 (2007).

[78] Y. Kim, W. Jeong, K. Kim, W. Lee, and P. Reddy, Nature Nanotech. **9**, 881 (2014).

[79] L. A. Zotti, M. Bürkle, F. Pauly, W. Lee, K. Kim, W. Jeong, Y. Asai, P. Reddy, and J. C. Cuevas, New J. Phys. **16**, 015004 (2014).

[80] S. Bedkihal , M. Bandyopadhyay, and D. Segal, Eur. Phys. J. B **86**, 506 (2013).

[81] E. Wierzbinski, R. Venkataramani, K. L. Davis, S. Bezer, J. Kong, Y. Xing, E. Borguet, C. Achim, D. N. Beratan, and D. H. Waldeck, ACS Nano **7**, 5391 (2013).

[82] H. A. Kramers, Physica **7**, 284 (1940).

[83] P. Rebentrost, M. Mohseni, I. Kassal, S. Lloyd, and A. Aspuru-Guzik, New J. Phys. **11**, 033003 (2009).

[84] V. Mujica, A. E. Roitberg, and M. A. Ratner, J. Chem. Phys. **112**, 6834 (2000).

[85] G. C. Liang, A. W. Ghosh, M. Paulsson, and S. Datta, Phys. Rev. B **69**, 115302 (2004).

[86] J. M. Beebe, B. Kim, J.W. Gadzuk, C. D. Frisbie, and J. G. Kushmerick, Phys. Rev. Lett. **97**, 026801 (2006).

[87] J. M. Beebe, B. S. Kim, C. D. Frisbie, and J. G. Kushmerick, ACS nano **2**, 827 (2008).

[88] T. Markussen, J. Chen, and K. S. Thygesen, Phys. Rev. B **83**, 155407 (2011).

[89] A. Vilan, D. Cahen, and E. Kraisler, ACS Nano **7**, 695 (2013).

[90] A. Landau, L. Kronik, and A. Nitzan, J. Comput. Theor. Nanosci. **5**, 535 (2008).

[91] R. Liu, S.-H. Ke, H. U. Baranger, and W. Yang, J. Chem. Phys. **122**, 044703 (2005).

[92] M. G. Reuter, G. C. Solomon, T. Hansen, T. Seideman, and M. A. Ratner, J. Phys. Chem. Lett. **2**(14), 1667 (2011).

[93] M. G. Reuter, T. Seideman, and M. A. Ratner, Nano Lett. **11**(11), 4693 (2011).

[94] M. G. Reuter, M. C. Hersam, T. Seideman, and M. A. Ratner, Nano Lett. **12**, 2243 (2012).

[95] L. Simine, W. J. Chen, and D. Segal, arXiv:1412.6175

[96] B. Capozzi, J. Xia, O. Adak, E. J. Dell, Z.-F. Liu, J. C. Taylor, J. B. Neaton, L. M. Campos, and L. Venkataraman, Nature Nanotech. (2015).